



Joint Institute for Nuclear
Research

SCIENCE BRINGING NATIONS TOGETHER

FINAL REPORT ON THE INTEREST PROGRAMME

Optimization of the solid ISOL method for
volatile reaction products of heavy ion beam
reactions

Supervisor: Mr. Viacheslav Vedeneev , JRS,
FLNR, JINR Dubna, Russia

Student: Ebrahim Ahmed ,University Of
Alexandria, Egypt

Participation period:

Wave 9, (31 October - 10 December 2023)
Dubna, 2023

November 28, 2023

Contents

1	Introduction	4
2	MASHA setup	5
3	Components	5
3.1	Target box.	5
3.2	ECR Ion Source.	6
3.3	Hot Catcher and Diagnostic System.	6
3.4	Detection and Control System.	9
3.5	Optimization of operation of the mass-separator	9
4	ISOL Method.	10
5	Experiment Results.	10
6	Histograms for Hg.	12
6.1	Hg-180	12
6.2	Hg-181	13
6.3	Hg-182	13
6.4	Hg-183	14
6.5	Hg-184	14
6.6	Hg-185	15
6.7	Hg-Matrix	15
7	Histograms for Rn : $^{40}\text{Ar} + ^{166}\text{Er} \longrightarrow ^{(206-xn)}\text{Rn} + xn$.	16
7.1	Rn-201	16
7.2	Rn-202	16
7.3	Rn-203	17
7.4	Rn-204	17

7.5	Rn-205	18
7.6	Rn-Matrix	18
8	histograms for Rn : $^{48}\text{Ca} + ^{242}\text{Pu} \rightarrow (^{21x})\text{Rn}$	19
8.1	Rn-212	19
8.2	Rn-218	19
8.3	Rn-219	20
8.4	Rn-Matrix	20
9	Conclusion	21
10	Acknowledgments	21

Abstract

Mass-separator MASHA located at FLNR, JINR, integrating ISOL method, revolutionizes superheavy nucleus (SHE) studies by enabling mass identification with simultaneous decay chains study. Kinematic separators, commonly used due to short half-lives, lack mass information. It combines the ISOL method for creating and separating radioactive nuclei with traditional mass analysis techniques to enable the identification of the masses of newly synthesized nuclides across a broad mass range. In the present chapter, the upgrade of some parts of MASHA are described: target box (rotating target+hot catcher), ion source based on electron cyclotron resonance, and Optimization of operation of the mass-separator. This allows scientists to investigate the α -decays or spontaneous fission of these superheavy nuclei [1].

1 Introduction

The production and exploration of super-heavy elements (SHE) within the realm of nuclear physics have a deep-rooted connection with the development of advanced accelerator technologies. This historical journey began with the emergence of cyclotrons, notably at the Joint Institute for Nuclear Research (JINR) in Dubna, Russia, which played a pivotal role in pioneering this field. These early cyclotrons, with their capacity to accelerate light ions, granted researchers access to isotopes up to neon, providing the necessary intensity and energy for fusion reactions [2]. Within this context, the Mass Analyzer of Super Heavy Atoms (MASHA) assumes a critical role as an instrument meticulously designed to discern superheavy nuclei based on their masses. Simultaneously, MASHA enables the detection of α -decays or spontaneous fission events. It achieves this through the integration of the ISOL method for nuclide extraction from a hot catcher and classical mass-spectrometry techniques. This study presents the outcomes of two independent experiments aimed at determining the separation efficiencies of mercury isotopes. The first experiment involved measuring absolute cross-sections in xn -evaporation channels for the reactions $^{40}\text{Ar} + ^{144}\text{Sm}$ and $^{48}\text{Ca} + ^{142}\text{Nd}$. This method builds upon the well-established catcher-foil experiment, providing valuable insights into the intricacies of heavy element production and exploration. In the second experiment, we obtained isotope yields in the same reactions using the solid-state ISOL method, facilitated by the mass spectrometer MASHA. The ratio of cross-sections measured in these experiments enabled the extraction of the separation efficiencies for the selected isotopes [3].

2 MASHA setup

MASHA (mass analyzer of super heavy atoms) represents a cutting-edge instrument meticulously crafted and stationed at the Flerov Laboratory, Joint Institute for Nuclear Research (JINR) in Dubna. Its core mission is to achieve the precise separation and mass measurement of both nuclei and molecules with exceptional accuracy surpassing 10^{-3} . MASHA operates seamlessly across a broad mass range, spanning from approximately $A \simeq 20$ to $A \simeq 500$, boasting an impressive mass acceptance window of $\pm 2.8\%$. Notably, MASHA enables unambiguous mass identification of superheavy nuclei, achieving a remarkable resolution better than 1 atomic mass unit (*amu*) at the 300 amu level. Recent years have witnessed substantial upgrades to MASHA, enhancing its performance and capabilities. Key components such as the target box, ion source, data acquisition system, beam diagnostics, and control system have undergone thoughtful modifications to optimize functionality. This article delves into these recent enhancements, offering insights into the evolution of this cutting-edge instrument [4].

3 Components

The setup, the layout of which is shown in **Fig.1**, consists of the target assembly with a hot catcher; an ion source based on the electron cyclotron resonance (ECR); a magneto-optical analyzer (a mass spectrometer) composed of four dipole magnets (D1, D2, D3a, and D3b), three quadrupole lenses (Q1–Q3), and two sextupole lenses (S1, S2); and a detection system located in the focal plane of the spectrometer. The ion-optical scheme of the mass spectrometer was comprehensively considered in. In this section, we describe separate units of the setup and present results of measurements of the key separator characteristics [5].

3.1 Target box.

In **Fig.2a**, a schematic outlines the target+catcher system, employing rotating targets assembled into cassettes (**Fig.2b**) for enhanced efficiency and heat distribution. A photo in **Fig.2b** displays a target disc featuring ^{242}Pu , rotating at 25 Hz via a Siemens electric engine. Additionally, the division foil was replaced with a thin graphite foil for enhanced thermal stability compared to titanium foil. These strategic enhancements showcase a dedication to optimizing efficiency and ensuring the robustness of the experimental setup[4].

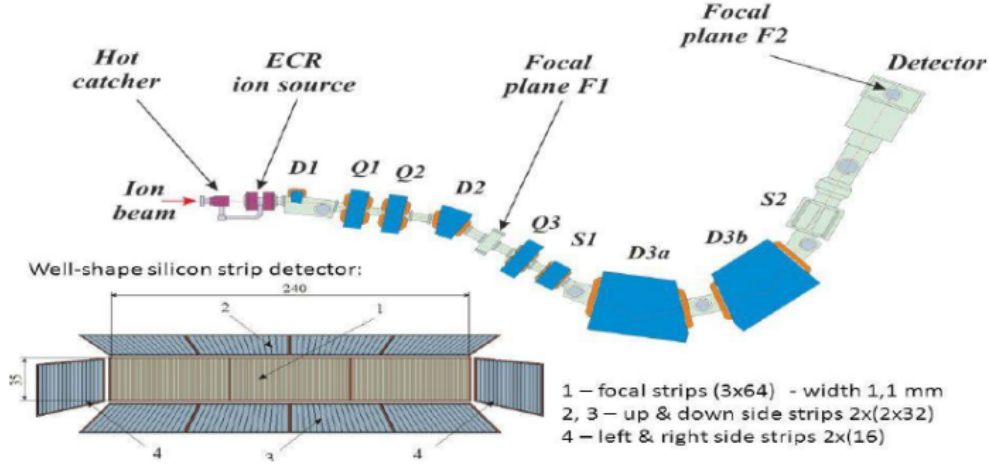


Fig.1: Schematic diagram of the MASHA mass separator: (D1, D2, D3a, D3b) dipole magnets, (Q1,Q2,Q3) quadrupole lenses, and (S1, S2) sextupole lenses. The detection system is in focal plane F2 of the separator.

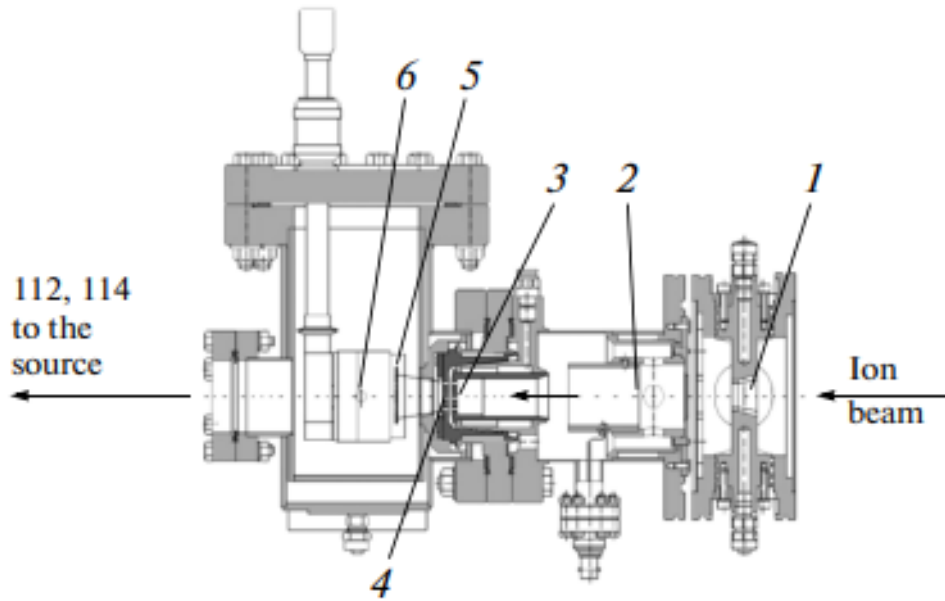
3.2 ECR Ion Source.

An ECR (Electron Cyclotron Resonance) ion source, operating at a frequency of 2.45 GHz , has been strategically chosen for the ionization of nuclear reaction products. Within the ECR, atoms undergo ionization to a charge state of $Q = +1$. Following ionization, a three-electrode system facilitates the acceleration of ions beam up to 38 keV , subsequently separated by the magneto-optical system within the mass spectrometer.

The ECR source is particularly effective in generating ion currents comprising nearly 100% singly ionized atoms, with a remarkable 90% ionization efficiency observed for noble gases(krypton, xenon) **fig.3**, we choose those gases because its first ionization potentials have maximum values and these are chemical inert elements. Operational parameters of the ECR source are finely tuned by optimizing microwave radiation power, frequency, and buffer gas pressure in the ionizer chamber. Helium, employed as a buffer gas, undergoes pressure regulation through a controlled piezoelectric valve. The source's optimal performance is achieved at a helium pressure ranging from $(1 - 2)10^{-5}\text{ mbar}$ and a microwave oscillator power of approximately 30 W . This careful calibration ensures the efficiency and accuracy required for ionization within the experimental setup [5].

3.3 Hot Catcher and Diagnostic System.

The hot catcher, an integral component of the target assembly depicted in **Fig 2**, is strategically positioned to intercept nuclear reaction products. Prior to reaching the target, the primary



b)



Fig.2: **a)**. Schematic overview of Target assembly with the hot catcher: 1 - split collimator; 2 - beam flux measuring foil; 3 - target; 4 - separating foil; 5 - graphite foil; 6 - heater. **b)**. The photo of the rotating target cassette in assembly. 6 packs, 2 windows at 14mm width each. Target material ^{242}Pu in oxide state put on the Ti 2 μm thick foil .

heavy-ion beam undergoes scrutiny in the diagnostic system. This system incorporates a split-type aperture comprising an electrostatic induction sensor and a Faraday cup. The split aperture, divided into four sectors, precisely measures the portion of the beam current not intercepted by the aperture hole, allowing for meticulous control of the beam position relative to the ion guide. The electrostatic induction sensor, a stainless steel tube fixed on an electrically isolated frame downstream of the split aperture, serves to monitor the current throughout the experiment. Simultaneously, the Faraday cup, positioned on a rotary vacuum-tight feedthrough 70 mm in front of the target, captures additional data on the beam characteristics.

These products traverse a separating foil and subsequently encounter a graphite absorber, heated

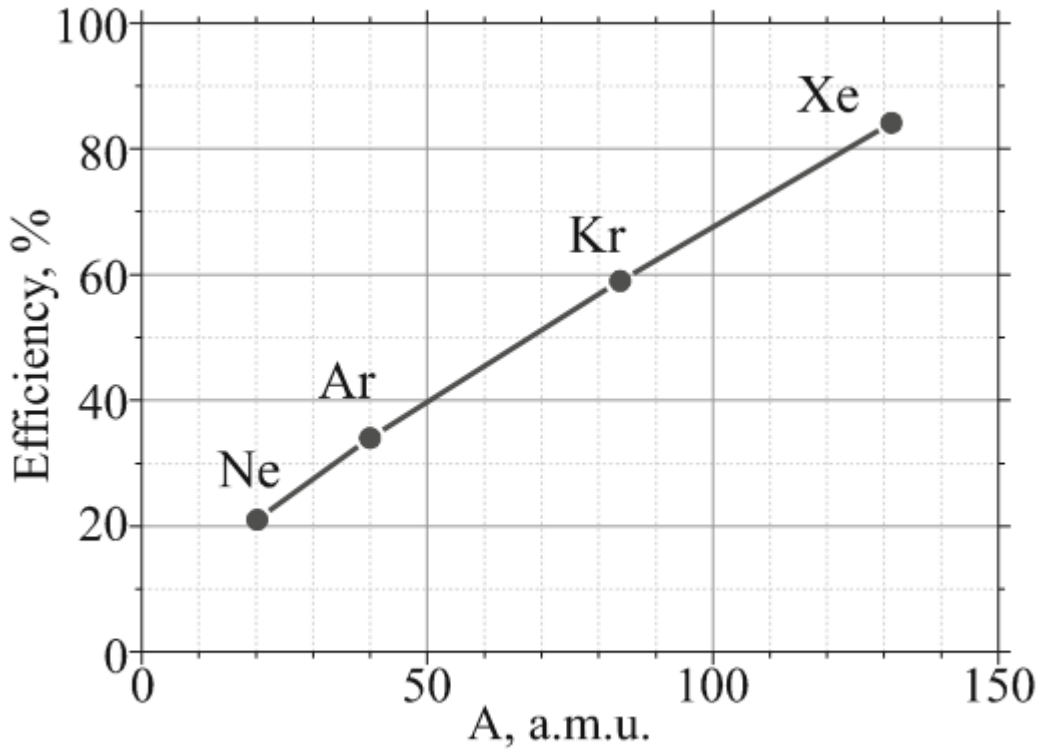


Fig.3: ECR ion source efficiency vs. mass number of noble gases

to a temperature range of $1800-2000K$. The foil of the thermo-expanded graphite with a density of 1.0 g/cm^3 and a thickness of 0.6 mm was used as a reaction product stopper. The stopper was a disk with a diameter of 30 mm . It was installed at a distance of 30 mm after the target. The graphite underwent heating as a result of the direct current flowing through it. The gap between the heater and the graphite stopper was 2 mm . The nuclear reaction products diffused in the form of atoms from the graphite into the vacuum volume of the hot catcher. Moving along the vacuum pipe, they reached the ECR ion source.

Temperature calibration of the graphite stopper, crucial for precise experimentation, is performed via an infrared pyrometer. This pyrometer, beyond the target's vacuum chamber, measures radiation from the heated graphite through a sapphire window. As the hot catcher's geometry prevents direct temperature monitoring during experiments, the required temperature is set based on the heater current. This well-calibrated setup ensures accurate control and measurement of thermal conditions, optimizing the study of nuclear reaction products in the experimental environment [2], [5].

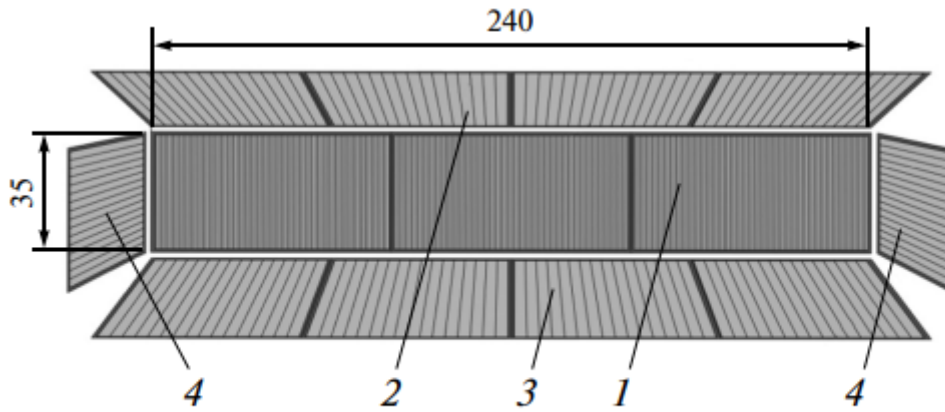


Fig.4: Focal plane silicon detector system: 1 - front detector; 2 - upper detector; 3 - lower detector; 4 - lateral detectors

3.4 Detection and Control System.

For detection of nuclear reaction products a silicon detector system was installed at the focal plane of the mass-separator (**Fig.4**). The front detector was a multi-strip copper structure fixed on the surface of glass-cloth laminate. It had an area of $240 \times 35 \text{ mm}$ and consisted of 192 strips with a pitch of 1.25 mm , and four additional detectors enhance geometrical efficiency. These detectors, each $300 \mu\text{m}$ thick, exhibit an entrance dead layer thickness not exceeding 50nm . The assembly allows for 90% detection of α -particles from a single nucleus decay in the front detector's center. A separate strip copper plate, akin to the front detector, measures small direct currents and aids ECR ion source tuning. Controlled by specialized multichannel electronic modules, the lower level of measured currents for each channel is 60 pA , with an upper level of $5 \mu\text{A}$. Signals from silicon detector strips are processed through spectrometric channels, leading to digital data transmission to a personal computer via a CAMAC standard. Electronic blocks, excluding preamplifiers, follow the CAMAC standard. Two independent software systems manage data collection and storage for the focal plane silicon detectors and the strip detector measuring small currents. The mass-separator's ion-optical elements, vacuum system, ECR ion source, and hot catcher are controlled using the LabVIEW packet on personal computers situated in the control room. This well-integrated setup enables comprehensive monitoring and analysis of nuclear reaction products[5].

3.5 Optimization of operation of the mass-separator

The optimization process for the ECR ion source and mass-separator operating modes involved calibrated leaks of noble gases added to helium buffer gas. These leaks supplied fluxes of about

$(1 - 3) \times 10^{-7} \text{ mbar} \times l/s$ of noble gas atoms, maintaining natural isotopic composition. In the absence of both the buffer gas and the microwave radiation the vacuum conditions allowed one to get in the discharge camera a pressure of $5 \times 10^{-7} \text{ mbar}$, predominantly helium (90 – 95%). About 3% of the flux comprised noble gas ions from the calibrated leak, with the remaining flux constituted by gas admixtures and ions generated by microwave plasma of the source. The mass spectrum of xenon isotopes measured. The obtained mass resolution determined at half-maximum of the peak $R = \frac{M}{\Delta M} = 1300$ (FWHM) appeared to be close to the result of the calculation [5].

Graphite stopper improvement:

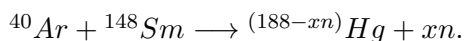
To stabilize separation efficiency in high-intensity beam experiments, a 0.6 mg/cm^2 graphene foil was added 2.5 mm before the main heater in the MASHA setup. This foil, heated by radiation, absorbs beam-induced heating load and acts as a barrier for low-energy reaction products. It prevents corruption of the "Hot Catcher," ensuring separation efficiency remains intact despite intense beams, averting over a fivefold reduction in just a few days. [6].

4 ISOL Method.

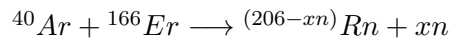
The Isotope Separation OnLine (ISOL) technique holds significant utility in the precise analysis of short-lived isotopes. This method relies on the controlled cooling and cessation of reaction products, enabling their subsequent analysis using magneto-optic and electrostatic means. Additionally, it facilitates their segregation from the primary beam in a continuous, uninterrupted "online" mode. At the MASHA facility, FLNR, JINR, the U-400M heavy ion beam was employed in an experiment to explore potential applications of novel carbon nanomaterials. The primary objective was to assess the resilience of these materials when subjected to the conditions required for the ISOL technique. Earlier investigations using a thermally expanded graphite heat catcher revealed its inadequacy in coping with high-intensity beams. Subsequent refinements in the ISOL methodology now permit the synthesis of new materials even at beam intensities reaching $0.5 \text{ p}\mu\text{A}$ and beyond, holding promise for the future operation of the Super-Heavy Element (SHE) factory.

5 Experiment Results.

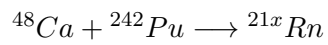
In this chapter isotopes of Hg are produced through fusion reaction.



Rn isotopes are produced through fusion reaction.

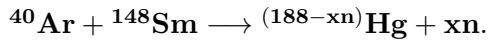


and multinucleon transfer reaction.



Alpha decays of the above isotopes are presented below. Decay energies are then analyzed in histograms and the experimental values using "Origin Pro software " are being compared to the theoretical expected values. In some charts the decay energy of the daughter nuclei is also observed. The last figure for each reaction resembles the heat map which is created by the silicon sensor after calibration with the respective energies from the histograms and chart of nuclides.

6 Histograms for Hg.



6.1 Hg-180

Hg 180 : Half Life: 2.58 sec & & ${}^{180}\text{Hg}$ decays by 48% at 6120 keV α -Decay energy level &
& ${}^{176}\text{Pt}$: Half life: 6.35 sec & & ${}^{176}\text{Pt}$ decays by 40% at 5750 keV α Decay energy Level.

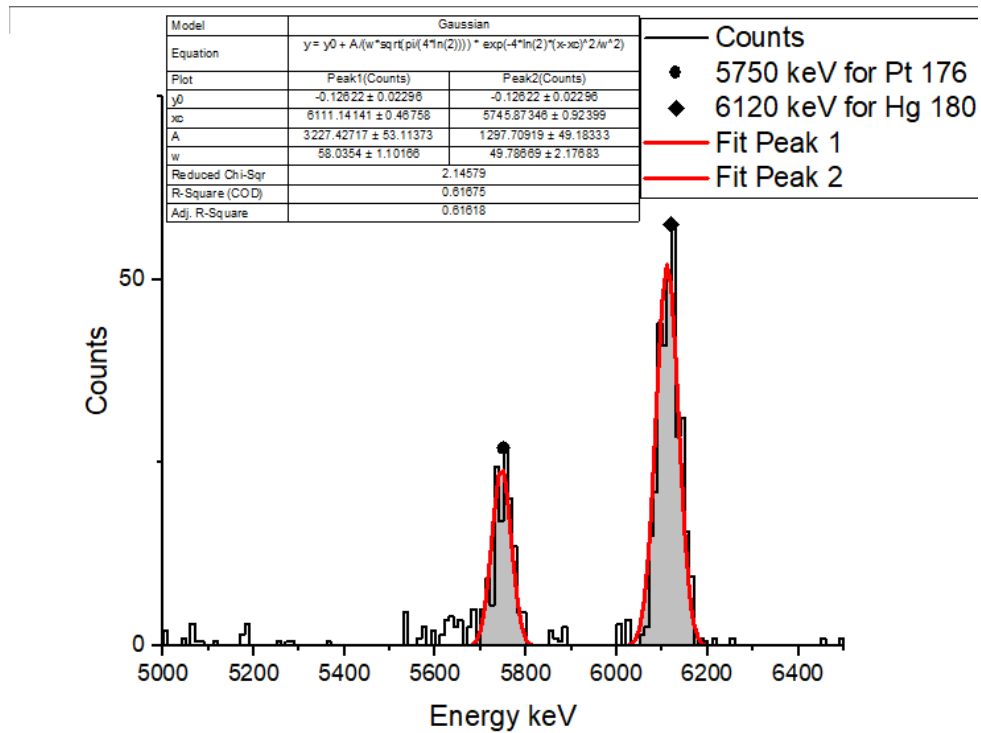
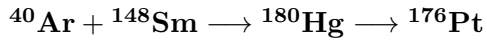


Fig.5: ${}^{180}\text{Hg}$ [2.58 s] decays with alpha energy 6120 keV [theor. 6119 keV - 99,9%].

6.2 Hg-181

Hg 181 : Half-Life: 3.5 sec & ^{181}Hg decays by 30 % at 6000 keV α - Decay energy level & ^{177}Pt : Half-life: 11 sec & ^{177}Pt decays by 5.6% at 5500 keV α -Decay energy Level.
 $^{40}\text{Ar} + ^{148}\text{Sm} \rightarrow ^{181}\text{Hg} \rightarrow ^{177}\text{Pt}$

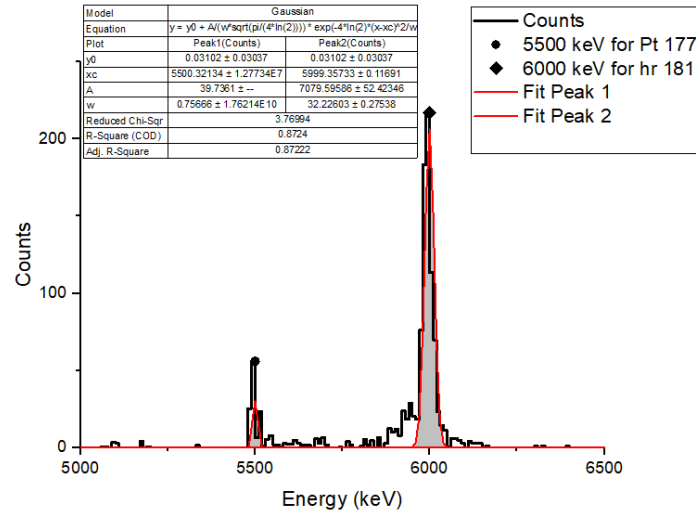


Fig.6: ^{181}Hg [3.54 s] decays with α -energy 6000 keV [theor. 6006 keV - 87%]

6.3 Hg-182

^{182}Hg : Half-Life: 10.835 sec & ^{182}Hg decays by 15.2 % at 5860 keV α -Decay energy level & ^{178}Pt : Half-life: 21.1sec & ^{178}Pt decays by 4.6% at 5450 keV α - Decay energy Level.
 $^{40}\text{Ar} + ^{148}\text{Sm} \rightarrow ^{182}\text{Hg} \rightarrow ^{178}\text{Pt}$

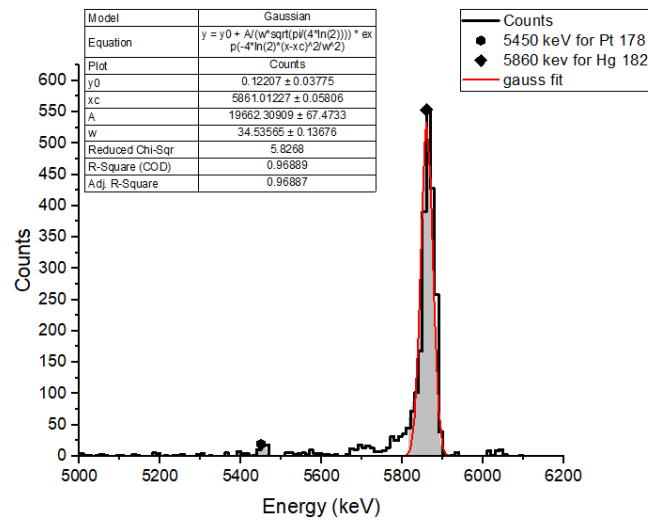


Fig.7: ^{182}Hg [10.83 s] decays with α - energy 5860 keV [theor. 5867 keV - 99%]

6.4 Hg-183

^{183}Hg : Half-Life: 9.4 sec & & ^{182}Hg decays by 11.7 % at 5890 keV α -Decay energy level & &

^{178}Pt : Half life: 21.1 sec & & ^{178}Pt : decays by 0.24 % at 5200 keV α -Decay energy Level.

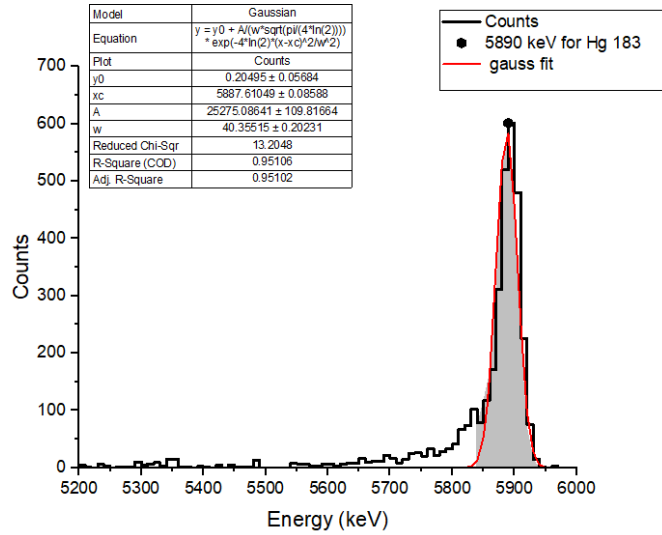
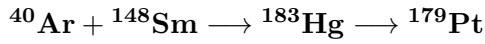


Fig.8: ^{183}Hg [9.4 s] decays with α - energy 5890 keV [theor. 5904 keV -91%]

6.5 Hg-184

^{184}Hg : Half Life: 30.9 sec & & ^{184}Hg decays by 1.26 % at 5530 keV α -Decay energy Level.

^{180}Pt : Half-life: 56sec & & ^{180}Pt decays by 0.3 % at 5140 keV α - Decay energy Level.

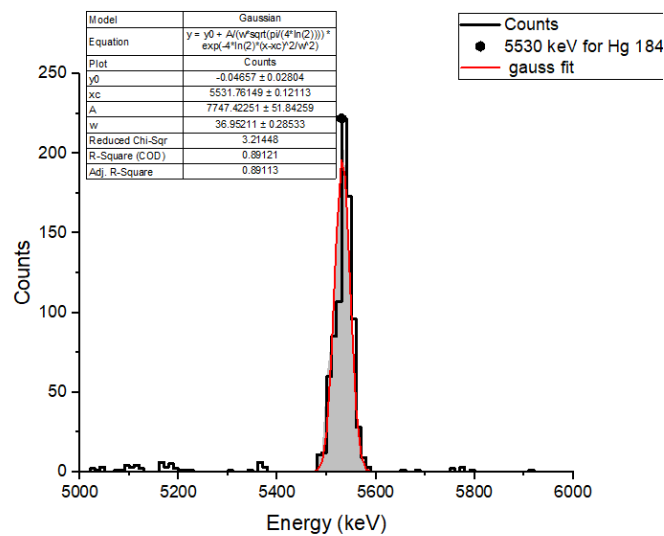
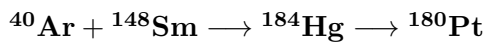


Fig.9: ^{184}Hg [30.9 s] decays with α - energy 5530 keV [theor. 5535 keV - 99.4 %]

6.6 Hg-185

^{185}Hg : Half Life: 49.1 sec & ^{185}Hg decays by 16 % at 5650 keV α -Decay energy Level & ^{181}Pt : Half-life: 52sec & ^{180}Pt decays by 0.074 % at 5080 keV α -Decay energy Level.
 $^{40}\text{Ar} + ^{148}\text{Sm} \rightarrow ^{185}\text{Hg} \rightarrow ^{181}\text{Pt}$.

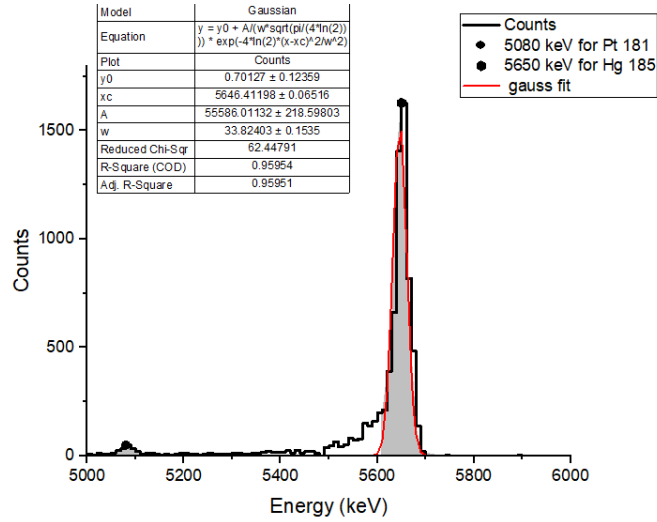


Fig.10: ^{185}Hg [49.1 s] decays with α - energy 5650 keV [theor. 5653 keV - 96%

6.7 Hg-Matrix

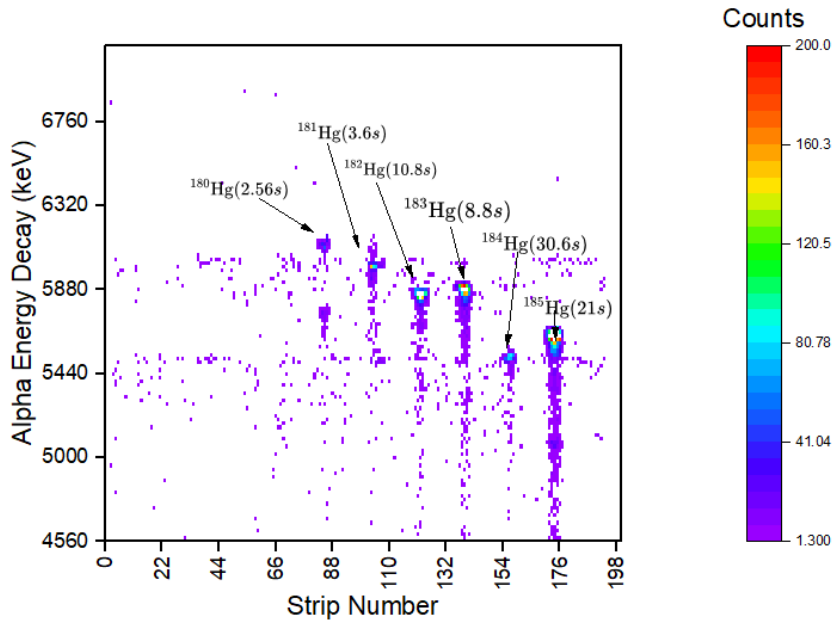


Fig.11: Heat map of Counts, $E_{\alpha\text{-decay}}$ and Strip number

7 Histograms for Rn : $^{40}\text{Ar} + ^{166}\text{Er} \longrightarrow (206-xn)\text{Rn} + xn.$

7.1 Rn-201

^{201}Rn : Hal-Life: 7.1 sec & ^{201}Rn decays by 80 % at 6760 keV α - Decay energy level & ^{197}Po : Half-life: 53.6 sec & ^{197}Po decays by 44% at 6380 keV α -Decay energy Level Also, Half-life: 25.8 sec ^{197}Po decays by 84% at 6380 keV α -Decay energy Level . $^{40}\text{Ar} + ^{166}\text{Er} \longrightarrow ^{201}\text{Rn} \longrightarrow ^{197}\text{Po} + ^4\text{He}.$

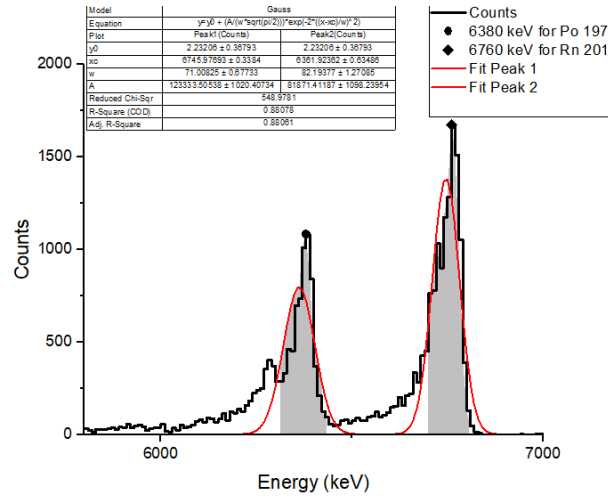


Fig.12: ^{201}Rn : [7.1 s] decays with α - energy 6760 keV [theor. 6725 keV]

7.2 Rn-202

^{202}Rn : Half-Life: 10 sec & ^{202}Rn : decays by 90% at 6630 keV α -Decay energy level & ^{198}Po : Half-life: 1.77 min & ^{198}Po decays by 57% at 6180 keV α - Decay energy Level. $^{40}\text{Ar} + ^{166}\text{Er} \longrightarrow ^{202}\text{Rn} \longrightarrow ^{198}\text{Po} + ^4\text{He}.$

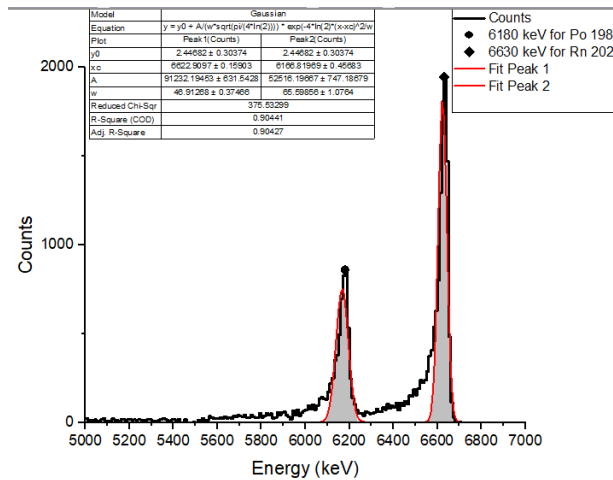


Fig.13: ^{202}Rn [7.1 s] decays with α -energy 6760 keV [theor. 6725 keV]

7.3 Rn-203

^{203}Rn : Half-Life: 45 sec & ^{203}Rn decays by 66 % at 6550 keV α - Decay energy level. ^{199}Po : Half-life: 5.48 min ^{199}Po decays by 12% at 6070 keV α - Decay energy Level.

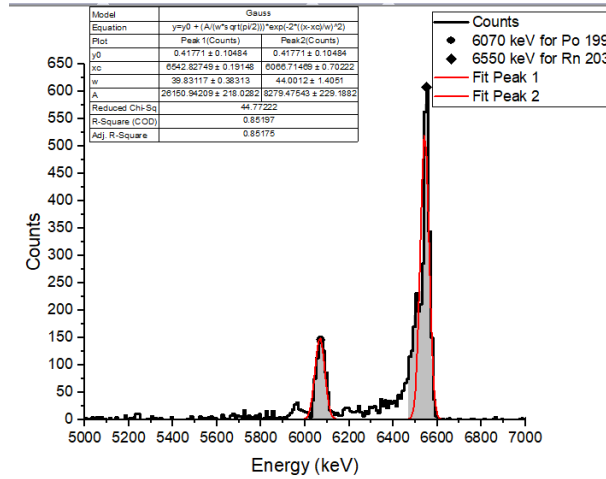
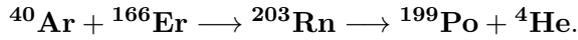


Fig.14: ^{203}Rn : [45 s] decays with α - energy 6550 keV [theor. 6499 keV -99%]

7.4 Rn-204

^{204}Rn : Half-Life: 1.24 min & ^{204}Rn decays by 73 % at 6400 keV α -Decay energy level. & ^{200}Po : Half-life: 11.5 min & ^{200}Po decays by 11% at 5860 keV α -Decay energy Level. $^{40}\text{Ar} + ^{166}\text{Er} \longrightarrow ^{204}\text{Rn} \longrightarrow ^{200}\text{Po} + ^4\text{He}.$

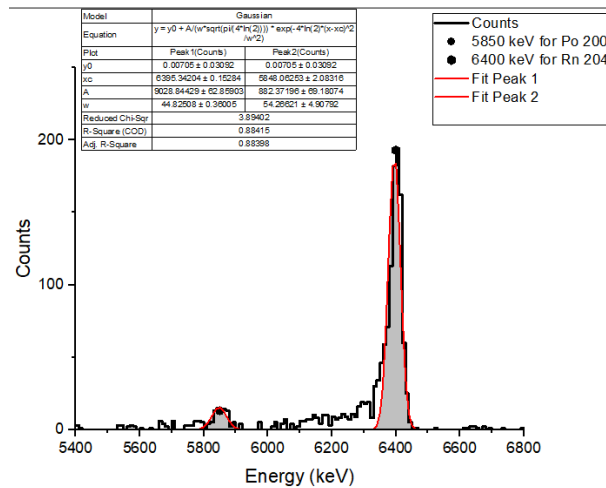


Fig.15: ^{204}Rn [74 sec] decays with α -energy 6400 keV [theor. 6418.9 keV].

7.5 Rn-205

^{205}Rn : Half-Life: 170 sec & ^{205}Rn decays by 23% at 6270 keV α - Decay energy level. & &

^{201}Po : Half-life: 15.3 min & ^{201}Po decays by 1.6% at 5910 keV α -Decay energy Level. $^{40}\text{Ar} + ^{166}\text{Er} \longrightarrow ^{205}\text{Rn}$

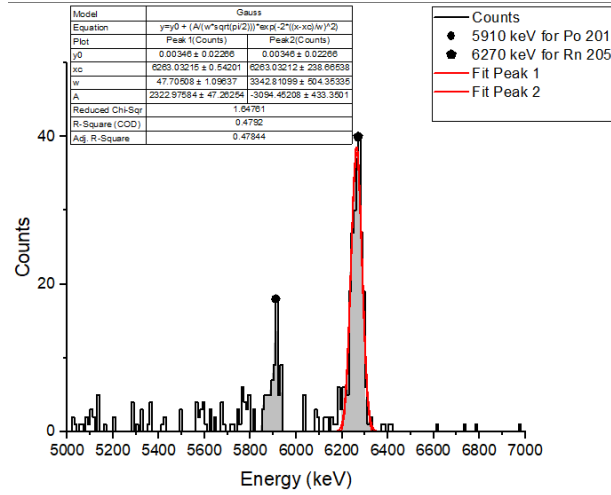


Fig.16: ^{205}Rn : [170 s] decays with α -energy 6270 keV [theor. 6262 keV - 98.2%].

7.6 Rn-Matrix

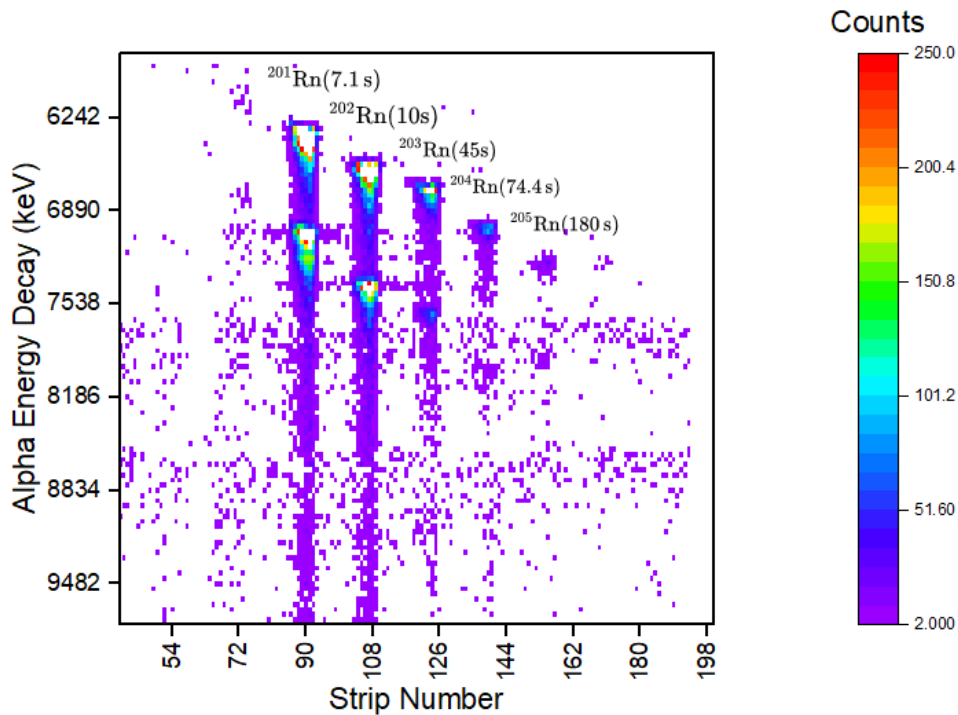


Fig.17: Heat map of Counts, E_α decay and Strip number.

8 histograms for Rn : $^{48}\text{Ca} + ^{242}\text{Pu} \longrightarrow (^{21x})\text{Rn}$

8.1 Rn-212

^{212}Rn : Half-Life: 23.9 min & & ^{212}Rn decays by 100% at 6250 keV α -Decay energy level & &

^{208}Po : Half-life: 2.898 years & & ^{208}Po decays by 99.99% at 5120keV α -Decay energy Level.:

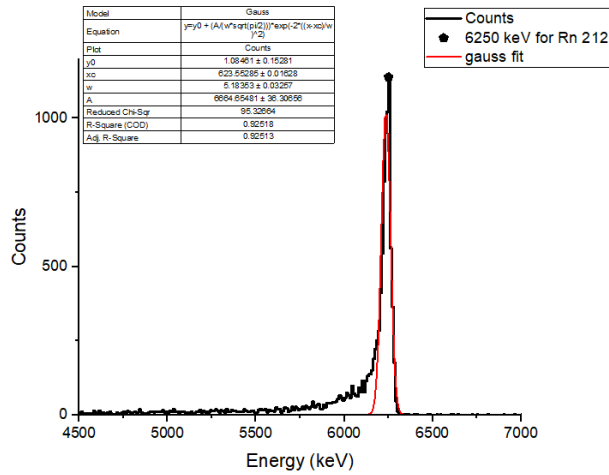
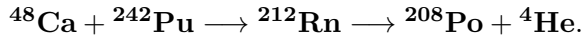


Fig.18: : ^{212}Rn [23.9 min] decays with α -energy 6250 keV [theor. 6264 keV].

8.2 Rn-218

^{218}Rn : Half-Life: 35 msec & & ^{218}Rn decays by 100% at 7110 keV α -Decay energy level

& & ^{214}Po : Half-life: 164.5 μsec & & ^{214}Po decays by 100% at 7660 keV α -Decay energy

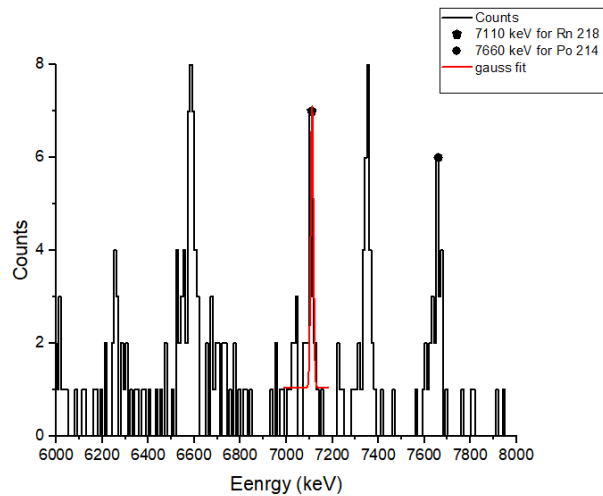
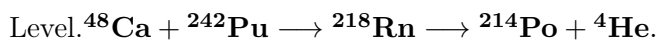


Fig.19: ^{218}Rn [35 msec] decays with α -energy 7110 keV [theor. 7129 keV].

8.3 Rn-219

^{219}Rn :Half-Life: 3.96 sec & ^{218}Rn decays by 100% at 6790 keV α -Decay energy level &

^{215}Po : Half-life: 1.781 msec & ^{215}Po decays by 100% at 7380 keV α - Decay energy Level.

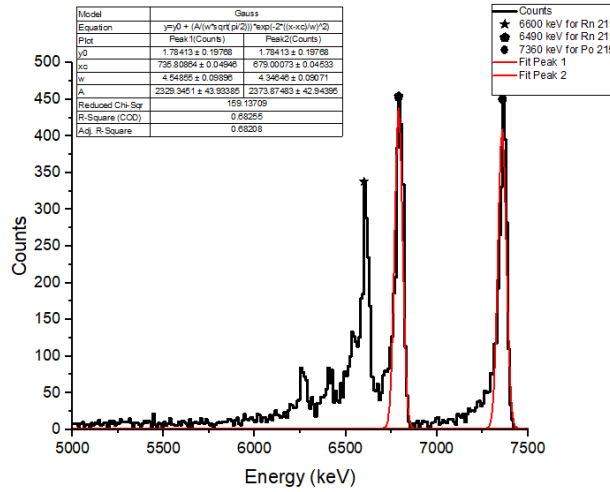


Fig.20: ^{219}Rn [3.96 s] decays with α -energy 6790 keV [theor. 6819 keV - 79.4%]

8.4 Rn-Matrix

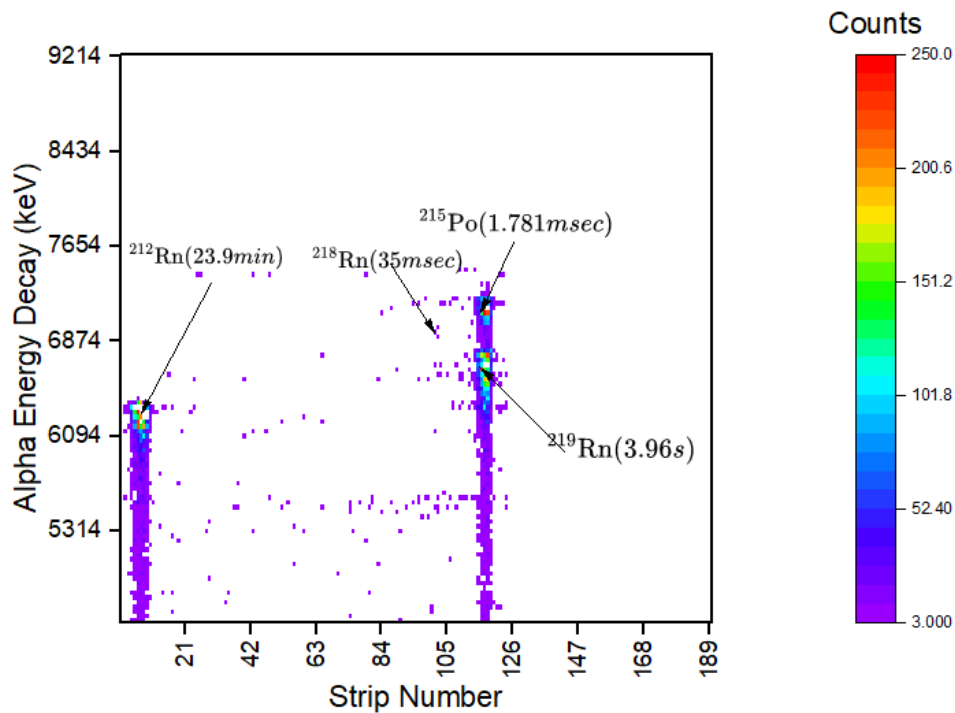


Fig.21: Heat map of Counts, E_α decay and Strip number.

9 Conclusion

In this study, we detailed the core components and operational sequence of MASHA. Since its initial installation, the system has undergone continuous enhancements. Our research at JINR aims to investigate Super Heavy Elements (SHEs) in pursuit of validating the theoretical concept of an 'Island of Stability,' hypothesized to harbor super heavy elements with remarkably extended half-lives compared to other elements. Utilizing the ISOL method, we generated a pristine beam of nuclei. Subsequently, employing a meticulously shielded and monitored setup, we conducted detailed observations of nuclear properties. The MASHA setup facilitated mass analysis, enabling precise separation of ions. Ongoing improvements to the entire facility have been a key focus, exemplified by the recent upgrade of the rotating target to carbon graphene nanotubes, significantly enhancing both separation efficiency and heat dissipation capabilities. Our comprehensive data analysis concerning nuclear fusions and multinucleon transfers demonstrated alignment with predicted theoretical values. The presented deviation error, ranging between 1-10 keV, remains within the expected norm, underscoring the reliability and accuracy of our findings.

10 Acknowledgments

I would like to thank the JINR institute and INTEREST team who organized this program as it was a great opportunity for me to extend my knowledge and enhance my experience regarding nuclear physics. I am grateful to my project supervisor Mr. Viacheslav Vedenev for his help through this workshop. His knowledge and attitude have inspired me to continue to try and become better at my field. I hope for an equally wonderful collaboration in a future project.

References

- [1] M. Schädel and D. Shaughnessy, *The chemistry of superheavy elements*. Springer, 2013.
- [2] A. Rodin, A. Belozerov, E. Chernysheva, *et al.*, “Separation efficiency of the masha facility for short-lived mercury isotopes,” *Hyperfine Interactions*, vol. 227, pp. 209–221, 2014.
- [3] E. Chernysheva, A. Rodin, S. Dmitriev, *et al.*, “Determination of separation efficiency of the mass-spectrometer masha by means of measurement of absolute cross-sections of evaporation residues,” pp. 386–390, 2020.
- [4] V. Y. Vedenev, A. Rodin, L. Krupa, *et al.*, “The current status of the masha setup,” *Hyperfine Interactions*, vol. 238, pp. 1–14, 2017.
- [5] A. Rodin, A. Belozerov, D. Vanin, *et al.*, “Masha separator on the heavy ion beam for determining masses and nuclear physical properties of isotopes of heavy and superheavy elements,” *Instruments and Experimental Techniques*, vol. 57, pp. 386–393, 2014.
- [6] A. Rodin, E. Chernysheva, S. Dmitriev, *et al.*, “Features of the solid-state isol method for fusion evaporation reactions induced by heavy ions,” in *Exotic Nuclei: Proceedings of the International Symposium on Exotic Nuclei*, World Scientific, 2020, pp. 437–443.